Chemical Engineering Journal 419 (2021) 129542

Contents lists available at ScienceDirect

Chemical Engineering Journal

journal homepage: www.elsevier.com/locate/cej

Photodegradation of textile pollutants by nanocomposite membranes of polyvinylidene fluoride integrated with polyaniline–titanium dioxide nanotubes

Hifza Nawaz [a,1], Muhammad Umar [a,1], Iqra Nawaz [b], Qasim Zia [a], Madeeha Tabassum [c], Humaira Razzaq [d], Hugh Gong [a], Xiubo Zhao [e], Xuqing Liu [a,*]

[a] Department of Materials, University of Manchester, Oxford Road, Manchester M13 9PL, United Kingdom
[b] Department of Biological Sciences, Pakistan Institute of Engineering and Applied Sciences, Islamabad 45320, Pakistan
[c] School of Engineering and Materials Science, Queen Mary University of London, Mile End Rd, London E1 4NS, United Kingdom
[d] Department of Chemistry, University of Wah, Rawalpindi 47040, Pakistan
[e] Department of Chemical and Biological Engineering, The University of Sheffield, United Kingdom

ARTICLE INFO

Keywords:
Polyvinylidene fluoride
Polyaniline
Titania nanotubes
Nanofiltration membrane
Phase inversion
Anti-fouling
Photodegradation

ABSTRACT

In this research article, the PVDF (polyvinylidene fluoride)–PANI (polyaniline)–titanium nanotube (TNT) based nanocomposite membranes were synthesised through phase inversion method. The composition and structural properties of nanocomposite membranes were characterised by X-ray photoelectron spectroscopy (XPS), Fourier-transform infrared spectroscopy (FTIR), X-ray diffraction (XRD), atomic force microscopy (AFM) and scanning electron microscope (SEM). The significant properties of synthesised membranes such as distribution of pore size, thermal properties, mechanical properties, and photocatalytic behaviour of membranes were also studied. The hydrophilic properties of the composite membranes increased with filler content (PANI-TNT) and results in improved pure water flux (484.8 ± 2.9 L/m^2 h^{-1}) compared to that (312.0 ± 1.91 L/m^2 h^{-1}) of the pure PVDF membrane. The pure PVDF and nanocomposite membrane were further analysed in terms of their filtration properties such as adsorption of dyes (methyl orange, Allura red) and UV self-cleaning properties. The newly developed nanocomposite membranes showed excellent pollutant removal efficiency (~90%). The synthesised nanocomposite membranes also showed photocatalytic activities due to the presence of TNTs, and adsorption of methyl orange (MO) reduces significantly with the UV light irradiations. The UV self-cleaning property of the composite membrane was further confirmed due to their high flux recovery ratio of about 94%. The results show that embedded PANI-TNT within nanocomposite was photo-catalytically active and degrade the dye molecules from the surface of the nano composite membrane.

1. Introduction

Water is essential for living organisms present on the earth. Human requires water for agriculture, drinking, washing and other living purposes. Out of all the water on earth, only 3% (freshwater) is considered suitable for the consumption of humans, the rest of water is in oceans with a large number of dissolved salts [1]. Freshwater is significantly affected by hazardous human activities which results in water pollution. Wastewater is categorised into municipal and industrial wastewater. Wastewater discharged from industries is more dangerous for the environment because it contains toxic chemicals, dissolved salts, and other organic, inorganic volatile compounds [2,3]. For example, textile industries use different chemicals for their processes, such as manufacturing yarns or cloths, seizing, and dyeing. Dyeing is the process of colouring the cloths, which mainly includes dyes along with a large quantity of water [4]. These dyes are dissolved into water and then fixed on clothes with the help of compounds called fixers. The remaining water is considered as the wastewater which directly discharges in

* Corresponding author.
E-mail addresses: hafizahifza.nawaz@postgrad.manchester.ac.uk (H. Nawaz), muhammad.umar@manchester.ac.uk (M. Umar), qasim.zia@manchester.ac.uk (Q. Zia), m.tabassum@qmul.ac.uk (M. Tabassum), humaira.razzaq@uow.edu.pk (H. Razzaq), hugh.gong@manchester.ac.uk (H. Gong), xiubo.zhao@sheffield.ac.uk (X. Zhao), xuqing.liu@manchester.ac.uk (X. Liu).
[1] These authors contributed equally.

https://doi.org/10.1016/j.cej.2021.129542
Received 12 January 2021; Received in revised form 11 March 2021; Accepted 23 March 2021
Available online 29 March 2021

watercourses [5]. This wastewater includes many dissolved and undissolved impurities like unused dyes, dissolved salts, and dye fixers along with some heavy metal ions and carcinogenic materials. Nowadays, the emission of these dyes and chemicals is of great concern as they are causing a lot of environmental hazards [6,7]. Therefore, textile wastewater treatment is required to remove carcinogenic dyes for a sustainable environment [8].

Membranes are thin and porous sheets of material which can selectively separate contaminants from water when a driving force is applied [9]. In this process, selective components (dyes) are separated due to the affinity with the membrane material [10]. Membranes are commonly used for water purification through micro and nano filtration [11]. Polymer membranes are being used from last few decades for water filtration [12]. Membranes can be prepared by sintering, sol-gel, leaching techniques and phase inversion methods [13]. The phase inversion method is unique to produce asymmetric membranes which contain micro or nano-voids, pores and macro-pores [14].

Many PVDF polymer membranes are commercially available and are used for water filtration. Moreover, PVDF membranes have also been extensively used for scientific research and industrial processes due to their outstanding properties such as high thermal stability and good chemical resistance. However, the hydrophobicity of PVDF makes it prone to contamination by organic compounds which causes the decline of water flux due to enhanced fouling on surface of membranes [15]. Also, these membranes have the inherent low strength, which restricts their use in the industries. Therefore, elimination of these inherent shortcomings is of great interest for researchers. A lot of research work has been done to increase hydrophilicity and mechanical properties of PVDF based membranes. Guo et al. studied the various methods to counter the membrane fouling and membrane wetting by hydrophilic and hydrophobic modifications [16]. Later Feng et al. successfully separated volatile organic compounds from water by using PVDF nanofiber membrane. The overall mass transfer coefficient for chloroform through the nanofiber membrane was the highest recorded value for this purpose [17]. Xiao et al. investigated the use of PVDF microfiltration membranes prior to reverse osmosis process for reusing the reclaimed water. He conducted his study on secondary municipal effluent on the pilot-scale continuous filtration system. His work showed the possibility of using PVDF membranes for treating municipal wastewater [18].

Nanocomposite membranes with two or more different materials have gained the theoretical and technological interest of researchers due to the combined advantages of materials to obtain better performance. The organic nanomaterials are of great interest due to their certain functional groups and large surface area as compared to bulk materials [19]. Recently, membranes have been modified by using titanium dioxide (TiO_2) nanotubes; this modification usually result in change of shape and size of nanomaterials [20,21]. TiO_2 nanotubes have also shown several benefits such as higher surface area, high hydrophilic properties, improved photocatalytic activity, increased robustness and excellent mechanical stability [21,22]. X. Cao et al. studied the effect of titania nanoparticles on the PVDF membrane. It was found that the addition of TiO_2 nanoparticles has improved the self-cleaning properties of the membrane through photodegradation. The antifouling and permeability of the membranes were also significantly increased [23].

Polyaniline (PANI) is a special polymer due to its versatile properties such as easy preparation, high conductivity, chemical stability [24], nontoxicity, less cost, good steric hindrance and excellent separation properties [25]. Furthermore, it can also be used as substitute to improve hydrophilic characteristics of membranes due to its functional groups [26]. PANI based nanofibers also exhibit high hydrophilicity and surface area. So, they have been used to enhance hydrophilic characteristics of surfaces. Teli et al. [27] synthesised polysulfone/TiO_2 ultrafiltration nanocomposite membranes which shows enhanced antifouling and hydrophilic properties of membrane due to inclusion of TiO_2.

This research article focuses on the preparation of the nanocomposite membranes for effective removal of dye molecules from textile wastewater. TNTs can be used to enhance self-cleaning properties by photodegradation of pollutants adsorbed on the surface of membranes. PANI and TNT also improve the hydrophilic nature of the nanocomposite membrane which enhances the water flux of membranes. We used phase inversion method for the synthesis of pure PVDF and PVDF-PANI-TNT nanocomposite membranes and studied the effect of nanofiller (PANI-TNT) on membrane's morphology, efficiency, and filtration performance. X-ray photoelectron spectroscopy (XPS), thermogravimetric analysis (TGA), Fourier-transform infrared spectroscopy, Atomic force microscopy (AFM), scanning electron microscopy (SEM), X-ray diffraction (XRD) and universal testing machine were used to characterise the developed membranes. Meanwhile, the developed nanocomposite membranes were investigated for their permeation properties such as BSA rejection, porosity, shrinkage ratio, solvent contents, dyes rejection and water/dye flux. Moreover, the self-cleaning properties were studied under UV light to check the effect of photodegradation efficiency of novel nanocomposite membranes. To the best of our knowledge, no one has studied the combined effect of TNT and PANI on PVDF membrane, self-cleaning properties of PVDF-PANI-TNT membranes and their usage for textile wastewater treatment.

2. Experimental

2.1. Materials

Chemical include the poly (vinylidene fluoride) with a M.wt of 64.035 (Sigma-Aldrich), polyaniline (emeraldine salt) with a M.wt of 10000 g/mol (Alfa Aesar) *N,N*-Dimethyl formamide (DMF) (synthesis grade, 97% (scharlu), Sulphuric acid (H_2SO_4) (scharlu), 1-propanol extra pure (C_3H_8O, ≥99%) (scharlu), Hydrogen peroxide (H_2O_2), NaOH (Sodium hydroxide, ≥98%) membrane, Acetic Acid (CH_3COOH, ≥97%), Ethanol (C_2H_5OH, ≥99.08%) (AnalaR®) were used as received.

2.2. Synthesis of TiO_2 nanotubes

The sol-gel process was used to synthesise titania nanoparticles [28]. The mixing ratio of 7:2:1 of ethanol, acetic acid and water was used to prepare a solution. After that 5 mL titanium isopropoxide was added dropwise in prepared solution at constant temperature (60 °C) with continuous stirring in a closed container. Then the solution was stirred continuously for three hours to form the dope solution. Afterwards, dope solution was kept for agitation for 24 h until gel was formed. Vacuum oven was used to dry the gel at 60 °C for four hours. Then powder was grinded, sieved and calcined (for 5 h at 450 °C). Hydrothermal process [29] was used to convert titania nanoparticles to titania nanotubes. 5 g of TiO_2 was mixed with 20 mL (10 M) NaOH solution and continuously stirred at 160 °C for 5 days after keeping in Teflon-lined autoclave. The developed precipitate was white in colour, and it was washed with water (5 to 6 times) and 0.01 M HCl until the solution becomes neutralised. Vacuum oven was used to dry the product at 100 °C for 4 h. The formed powder was ground, sieved and calcined at 360 °C for 4 h.

2.3. Fabrication of PVDF-PANI-TNT nanocomposite membrane

Polyaniline and titanium nanotube based composite were developed through in-situ chemical oxidation reaction with aniline monomer, where APS (ammonium persulfate) was used as an oxidising agent [19]. TNTs (4 g) were suspended in 40 mL HCl (1 M) solution and sonicated for one hour. 50 mL Aniline (0.1 M) was added in prepared solution. Then 3 mL ammonium persulfate (1 M) was added dropwise with continuous stirring using ice bath [30]. The mixture was kept under constant stirring for five hours to polymerise the solution, and then it was filtered and further washed with ethanol and water several times. Fig. 1 schematically illustrates the process of manufacturing the

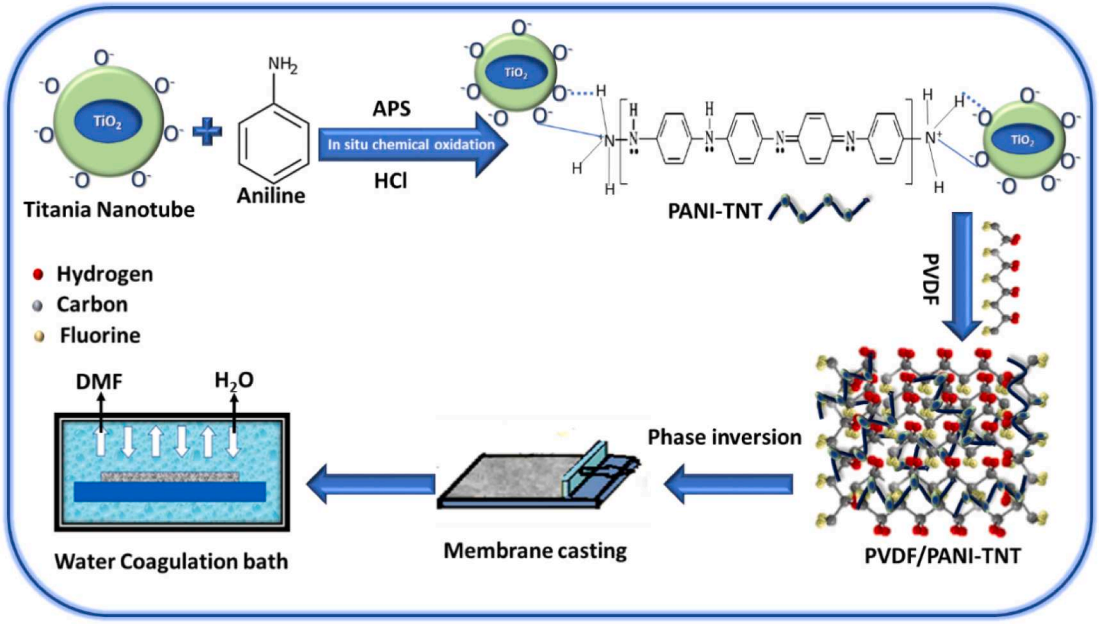

Fig. 1. Schematic illustrations of the manufacturing process of nanocomposite membrane.

nanocomposite membrane. As shown, oxygen molecules are adsorbed on the outer layer of titania nanotubes and generate O_2^-, O^{2-}, O^- ions, which results in positive charge on the surface of titania nanotubes by the emission of electron from titanium conducting bands [31]. When titania nanotubes were added in aniline solution, then the aniline monomer displays an electrostatic force of interaction with anion surface of titania nanotubes [32]. During polymerisation of aniline monomers, polyaniline slightly covers the surface of titanium nanotubes.

Phase inversion method was used to synthesise the PVDF-PANI-TNT nanocomposite membranes [33]. Firstly, the pure PVDF membrane was synthesised with DMF solvent. Different concentrations of PANI-TNTs (1 w/v % to 3 w/v %) were introduced to form composite membrane of PVDF-PANI-TNT. The resulting solution was sonicated for 2 h and stirred for 20 h. Then these prepared solutions were cast onto the glass plate substrate through hand casting knife, and then it was dipped immediately in the distilled water bath at 25 °C. After the process of phase inversion, synthesised membranes were left into the water bath for the extraction of remaining solvents entrapped in PVDF-PANI-TNT nanocomposite membranes. The compositions and codes are given in the Table 1.

2.4. Characterisation

Membranes were characterised by different techniques. The structural properties of samples were analysed by Panalytical 3040/60 X pert PRO diffractometer (XRD) using Cu (Kα) source in the range of 0θ to 80θ. The roughness of developed membranes was determined by using Atomic force microscopy. AFM micrographs were obtained with use of Bruker Multimode 8 AFM equipped with J scanner and Nu Nano Scout 350 probes in ScanAsyst mode. The data was processed with use of Gwyddion software (tilt correction). FTIR spectra obtained from 1000 Perkin Elmer within range of 400–4000 cm^{-1} was used to measure the functional groups of developed membranes. We investigate thermal stability of developed membranes by Thermal gravimetric analysis (TGA/DT Perkin-Elmer, USA). Surface and cross sectional morphology of prepared membranes were analysed by using SEM (VP-1450 Germany, LEO) with an accelerating voltage of 20 kV. XPS spectra were measured using a Kratos Axis Ultra instrument equipped with a monochromatic Al ka X-ray source (E = 1486.6 eV). A charge neutraliser was used to minimise charging and spectra are aligned on the binding energy scale relative to the hydrocarbon peak at 284.8 eV. Spectra were fitted using the CASA XPS software using Voigt-like peak shapes. Spin-orbit splitting ratios and splitting energies are constrained to obtain physically meaningful fits. Atomic composition of the samples was calculated from survey spectra with use of Shirley type background. The mechanical properties of developed membranes were measured by the universal testing machine.

Table 1
Codes of PVDF/PANI-TNT composite membranes.

Codes	PVDF W/V (%)	PANI-TNT W/V (%)	DMF W/V (%)	Total concentration
0P	15.00	0	85	100.0
PTP1	14.00	1	85	100.0
PTP2	13.00	2	85	100.0
PTP3	12.00	3	85	100.0

3. Study of membrane properties

To evaluate the effectiveness of composite membranes for the practical amplification in wastewater treatment, the following permeation properties of membranes were analyzed.

3.1. Porosity

Gravimetric method was used for the determination of tiny holes within the structure of nanocomposite membranes which also defines their porosity. Membranes samples of dimension 1 cm^2 were dipped into the deionised water for 1 day [34]. The weight of membranes before and after saturation with water was measured. Porosity of developed membranes was calculated by using the following formula:

$$\text{Porosity}(\%) = \frac{(W_2 - W_1)/\rho w}{W_1/\rho m} \times 100$$

ρ_w represent the density of water and ρm represent the membrane density while W_1 is the weight before wetting and W_2 represent the weight after wetting of membrane.

3.2. Solvent content

The quantity of any solvent in membranes is referred to as solvent content which was evaluated by the same method used for porosity [35]. The membranes were dipped in solvents (water, methanol, ethanol and propanol) for 1 day. The membranes were weighed before and after saturation with solvents and following formula is used to calculate it.

$$\text{Solvent content}(\%) = \frac{W_2 - W_1}{W_2} \times 100 \quad (2)$$

W_1 is the weight before wetting and W_2 represent the weight after wetting of membrane.

3.3. Shrinkage ratio

Shrinkage ratio is defined as the volume of dry membranes to that of wet membranes. For the determination of shrinkage ratio, these membranes were cut into square piece (area = 1 cm^2). Then we dipped these pieces of membrane into the distilled water for 1 day. Their length, width and thickness were measured before and after saturation with water. For calculating shrinkage, the following formula was used:

$$\text{Shrinkageratio}\% = \left[1 - \frac{(a \times b \times d)}{(a_o \times b_o \times d_o)}\right] \times 100 \quad (3)$$

d_o is thickness, a_o is the length, and b_o is the width of wetted membranes, however thickness of dry membranes is represented by 'd' while length and width are represented by a and b respectively.

3.4. Water flux

The quantity of water which flows across the developed membrane per unit area and time in the presence of trans membrane pressure is pure water flux [36]. For determining water flux, the developed membranes were subjected to steady-state high pressure of approximately a few milli-bars. The formula used for the permeability calculation is as follow:

$$\text{Pure Water Flux}(J) = \frac{Q}{At} \quad (4)$$

Symbol 't' represent time, 'A' is area developed membrane (cm^2) while 'Q' is the quantity of water which passes through the composite membrane within 1 min.

3.5. Antifouling properties

Bovine serum albumin (BSA) is a model protein for the calculation of antifouling properties of the nanofiltration membrane. Initial pure water flux (Jw1) was measured by passing the BSA aqueous solution (0.80 g/L) through the filtration cell for half hour at 0.1 MPa. Then, the fouled membranes were washed with deionised water by dipping it into the water bath for 60 min. After cleaning, we calculate the pure water flux (Jw2) again [37]. The flux recovery ratio of synthesised membranes was evaluated by using the following formula.

$$FRR\% = \frac{J_{W1}}{J_{W2}} \times 100\% \quad (5)$$

For the rejection (per cent) of BSA [38], we used the following formula,

$$\text{Dyerejection}(\%) = \left(1 - \frac{C_P}{C_f}\right) \times 100 \quad (6)$$

C_p represents molarity of permeate solution, C_f represent molarity of feed solution. To measure the λ_{max} (280 nm) of permeate and feed solution, UV-vis spectrophotometer was used.

3.6. Determination of the dyes removal efficiency

For the evaluation of removal efficiency of synthesised membranes, two model dyes Allura red (AR) and methyl orange (MO) were used under the vacuum filtrations. The sample solutions (before and after the filtration) were analysed through UV-vis spectrophotometer (DR5000, Hatch). For the calculation of dyes concentration in the sample solution, UV spectrometer detect the wavelength of maximum absorbance. Following formula was used for the analysis of dyes rejection,

$$R(\%) = \left(1 - \frac{C_P}{C_f}\right) \times 100\% \quad (7)$$

C_p represents the molarity of the permeate solution, and C_f represent the molarity of feed solution. Calibration curves of model dyes (Allura red (λ_{max} = 505 nm) and methyl orange (λ_{max} = 464 nm)) are shown in Supplementary Data (Fig. S3). For the determination of dye removal (%) efficiency of synthesised membrane, we analysed our dyes solutions through fitting standard plot; (y = -0.7406 + 23.81x for Allura Red) and (y = -0.4317 + 9.715x for Methyl orange).

4. Results and discussion

4.1. Characterization of polyaniline titania nanotube composite

The sol-gel method was used to synthesis TiO_2 NPs and convert it into TNTs by hydrothermal process. The morphology of Titania nanoparticles and Titania nanotubes (TNT) was observed by SEM Fig. 2(A and B) respectively. As shown in Fig. 2(A), the size of TNPs is smaller than 1 μm. Fig. 2(B) demonstrates that the Titania nanotubes (TNT) have a tubular structure. The agglomeration was clearly observed that may occur due to the effects of the drying process. The average length of titania nanotubes were a few hundreds of nanometres. The synthesized TNTs were resembled to report by Abulhassan and colleagues [39]. Fig. 2(C and F) show that polyaniline is attached to the outer surface of the titania nanotube. Coating of polyaniline on TNT is multilayer aggregations. XRD results in Fig. 2(D) represents that the sample of TiO_2 nanoparticles illustrate five sharp characteristic peaks at 24.30°, 36.76°, 45.15°, 52.78° and 62.75° that correspond to the crystalline planes of (1 0 1), (0 0 4), (2 0 0), (1 0 5), (2 1 1) and (1 1 8) respectively. These were in excellent agreement with the reference (00–021-1272) of the joint committee on powder diffraction standards database [40]. According to Fig. 2(E), TNTs are synthesised into the anatase form. The significant peaks at 10.05°, 36.76°, 45.15°, 52.78°, 62.75° and 75.43° confirms the synthesis of titania nanotube. Fig. 2(G) illustrate the XRD analysis of the PANI-TNT composite. The graph shows that the intensity of peaks decreases due to the presence of amorphous polyaniline which weakens the diffraction peak of the titania nanotube. The crystallinity of titania nanotube was affected due to the agglomeration of polyaniline on their surfaces [41]. Fig. 2(H) show the FTIR analysis of the PANI-TNT composite. The peak at 676 cm^{-1} correspond to the vibration peak of the TiO_2 nanotube. Due to the presence of polyaniline within the composite, a broad peak at 1411 cm^{-1} shows the bending of the N-H group, 871 cm^{-1} correspond to the aromatic rings and at 1252 cm^{-1} represent the stretching modes of C-N on benzoic rings. EDX analysis was also performed to determine the elemental composition of the PANI-TNT composite. Fig. 2(I) illustrates the presence of Ti, C, O and N, which also confirms the synthesis of polyaniline–titania nanotube composite. These characterisations give clear evidence on synthesis of homogenous PANI-TNT composite.

4.2. Surface morphology of synthesised membranes

Scanning Electron Microscopy was used for analysing the surface morphology of pure PVDF and PVDF-PANI-TNT composite membranes. Fig. 3(A1–D1) represent the SEM images of developed pristine PVDF and

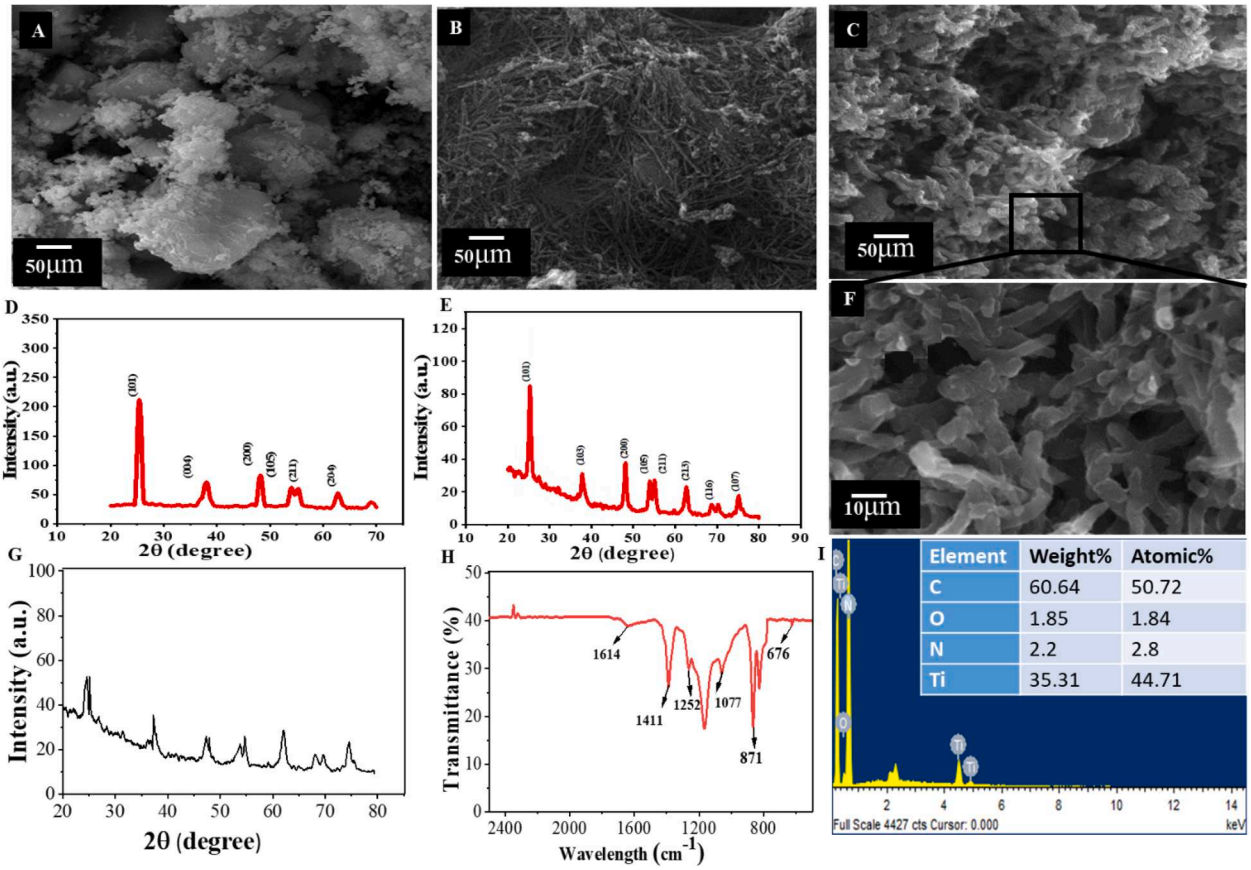

Fig. 2. (A) SEM image of titania nanoparticles. (B) SEM image of titania nanotubes. (C) SEM image of polyaniline–titania nanotube composites. (D) XRD analysis of titania nanoparticles. (E) XRD analysis of titania nanotubes. (F) Close up of polyaniline– titania nanotube composites. (G) XRD analysis polyaniline–titania nanotube composite. (H) FTIR analysis polyaniline–titania nanotube composite. (I) EDX analysis of polyaniline–titania nanotube composite.

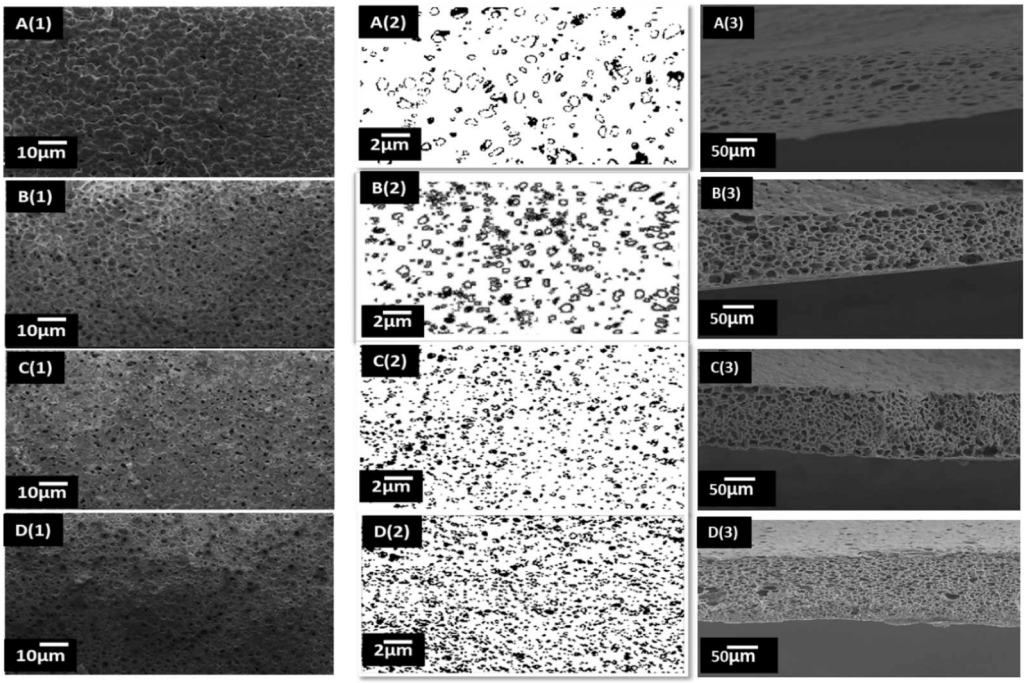

Fig. 3. Surface morphologies of pure PVDF membrane (A), PTP1 membrane (B), PTP2 membrane (C) and PTP3 membrane (D).

nanocomposite membrane's surfaces with various concentrations of polyaniline and titania nanotubes (PTP1, PTP2 and PTP3). SEM images of the synthesised membrane represent that the roughness and asymmetry on the membrane's surface enhance with the increase in the concentration of PANI-TNT within nanocomposite membranes. The membrane's surfaces also showed porous structures [42]. When the casting solution is immersed in a coagulation bath, the DMF from the casted membrane was exchanged with water from a coagulation bath. Thus, the membrane becomes porous due to the relative diffusion of DMF and deionised water [14].

Geometric analysis of SEM images represents the porous structure of the synthesised membranes. Image J software was used to regenerate the size and shape of pores within the membranes [43]. Fig. 3(A2–D2) shows the distribution of the pores with an estimated diameter of pores on the surface of the synthesised membrane. The analyses represent that filler (PANI -TiO_2) content increased the number of pores and decreased the pore's diameter in comparison to synthesised PVDF membrane, the pores are not equally distributed throughout the surface of the membrane and contain a relatively large pore diameter (about 1.53 μm) [44]. However, the average pore diameter of nanocomposite membranes (PTP1, PTP2, and PTP3) was 0.58(μm), 0.14(μm) and 0.009(μm), respectively. The Pore size of nanocomposite membrane was reduced due to excellent compatibility of filler content (PANI-TNT) with polyvinylidene difluoride [44]. The average diameter of pores in composite membranes decreases which improve the performance of membranes due to their excellent sieving mechanism [42]. The graphs of pore size distribution are shown in Fig. S2 (Supplementary Material). Fig. 3 (A3–D3) show the cross-sectional images of developed PVDF and nanocomposite PVDF/PANI-TNT membranes. Results conclude that developed composite membranes show the excellent miscibility of polymers (PVDF, PANI) and titania nanotubes, so these images do not show phase separation throughout the membrane structure [45]. Cross-sectional images represent the asymmetric morphology of pores within developed membranes. The thickness of synthesised membranes was about 100–150 μm. Fig. 3(A3) show that pure PVDF membrane has dense upper surface, which may be due to fast phase inversion into the distilled water (coagulation bath). Composite membranes PVDF/PANI-TNT in Fig. 3(B3–D3) membranes show more porous texture with uniform pores distribution throughout composite membranes. 3D AFM analysis was done within range of a 20 μm × 20 μm area of scan to measure the surface roughness of developed membranes. Fig. 4(A, B) represent the AFM analysis of developed membranes, which conclude that the R_a value of pure PVDF membrane is smaller (54.8 nm) than developed composite membrane (554.3 nm). The RMS value of developed composite membranes is also higher (649.8 nm) than pure PVDF membrane (68.1 nm). It confirms that surface roughness effectively increases to enhance the area of filtration which directly increase the pure water flux of composite membranes [2].

4.3. Surface composition of PVDF-PANI-TNT composite membranes

XRD diffractograms were also used for the determination of the purity and the crystallinity of PVDF-PANI-TNT nanocomposite membranes. XRD analysis of the pure PVDF and PVDF-PANI-TNT nanocomposite membrane with various concentration of TNTs was performed and the resulting graphs of composite membranes are plotted in Fig. 4(C). The spectra of pristine PVDF membrane show its characteristic α peaks at 12.08°, 20.4° and 35.11°. XRD diffractograms of TNT-PANI containing membranes illustrated that the individual peak of titania nanotube disappeared due to the amorphous nature of

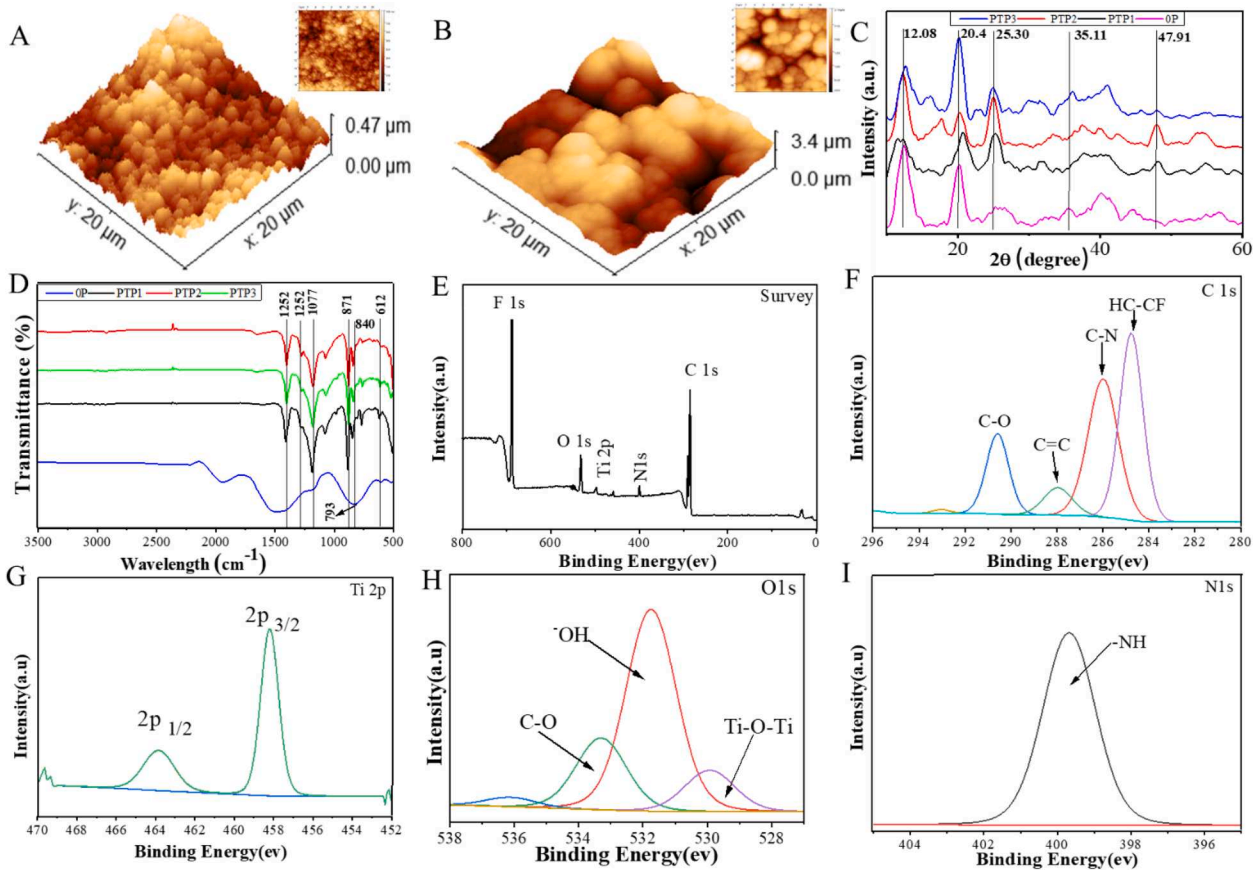

Fig. 4. (A) AFM images of pure PVDF membrane. (B) AFM images of PVDF/PANI-TNT composite membrane. (C) XRD graphs of PVDF/PANI-TNT composite membrane (D) FTIR of PVDF-PANI-TNT composite membrane. (E) XPS analysis of PVDF/PANI-TNT composite membrane. (F) C1s spectrum of the composite membrane. (G) Ti2p spectrum of the composite membrane. (H) O1s spectrum of the composite membrane. (I) N1s spectrum of the composite membrane.

membranes and showed a hump at about 25.30°, 37.76° and 47.91° [46]. Due to the crystalline nature of titania nanotube, α-phase peaks at 10.08° was disappeared in nanocomposite membranes while a new peak at 20.5° appears that correspond to (2 0 0) and (1 1 0) planes at β-phase. These β-polymorph represent the chemical interactions of —C═O (carbonyl groups) present in nanocomposite (TNT-PANI) and the C —F groups in polyvinylidene difluoride. These similar patterns of XRD peaks of composite membrane were shown for different concentrations of filler (PANI-TNT). But with increasing the concentrations of filler content, we can observe a small shift within the positions of hump.

Fig. 4(D) show the FTIR spectra of the synthesised membranes, which also confirmed the transformation of β-phase within the composite membranes (PVDF-PANI-TNT). Some characteristic peaks of PVDF appear in both composite membranes and pristine PVDF membrane at 792 cm^{-1} and 612 cm^{-1} which corresponds to CF_2 bending and CH_2 group respectively. All these peaks correspond to α-phase of synthesised PVDF membrane. While the XRD diffractograms of nanocomposite membrane shows the peak at 1077 cm^{-1}, 1271 cm^{-1} and 840 cm^{-1} which represents the β-phase of the PVDF-PANI-TNT membrane. Due to the presence of polyaniline within the composite membrane, a broad peak at 1411 cm^{-1} show the bending of N —H group, 871 cm^{-1} correspond to the aromatic rings and at 1252 cm^{-1} represent the stretching modes of C —N on benzoic rings [45]. In FTIR analysis, there are no significantly difference in peaks at different concentration of filler contents within the synthesised nanocomposite membrane but the intensities of these composite membrane has a small change due to the restriction of vibrations with the incorporation of various concentration of titania nanotubes [47]. XPS analysis of PVDF/PANI-TNT composite membrane was also performed for the identification of chemical states on the membrane surface. Fig. 4(E) show the survey XPS spectra of C1s, N1s, Ti2p, O1s and F1s. C1s spectra of the composite membrane is shown in Fig. 4(F). Two major peaks of HC-CF and C —N are shown at 284.2 and 285.6 (eV) respectively which confirm the presence of benzenoid rings of polyaniline and PVDF on the membrane surface. Less intense C=C peak at 288 (eV) represents the polymer chain of PVDF polymer. The peak of C —O shown at 290.8 (eV) corresponds to the linkage of composite (PANI-TNT) and PVDF [48]. Fig. 4(G) illustrate the characteristic peaks of Ti at 458 and 464 (eV). Fig. 4(H) show the characteristic peak of oxygen atom. Low intense peak at ~ 530 eV represents Ti —O —Ti. However, the peak at 531.6 eV and 533.7 eV correspond to ¯O —H and O —C bond [49].Therefore, XPS analysis provides evidence of surface elemental compositions and chemical states of the developed composite membrane.

4.4. *Mechanical stability and thermal of PVDF-PANI-TNT nanocomposite membranes*

To evaluate the mechanical properties of PVDF and nanocomposite PVDF-PANI-TNT membranes, Young's Modulus and tensile strength were determined and shown in Fig. 5(A, B). By adding the nanocomposite (PANI-TNT), nanocomposite membranes become brittle, but these membranes were stronger than pure PVDF membrane. PANI-TNT entangle with the chain of PVDF that provide some extra binding sites for the membranes, and it shows the excellent compatibility between the filler and PVDF [50]. Due to these interactions, tensile strength and young's modulus enhanced from 80.13 (MPa) to 178.04 (MPa) with the addition of nanocomposite (PANI-TNT). This increase in tensile strength of nanocomposite membranes is due to the presence of nanocomposite (polyaniline and titania nanotube), which contains a large surface area. It increases the molecular interactions between polyvinylidene fluoride and nanocomposite which is also proved by FTIR analysis. These mechanical properties of nanocomposite membrane shows good miscibility of filler content (PANI-TNT) with polyvinylidene fluoride [51]. The pressure resistance of the developed nanocomposite membranes was also tested, and results are discussed in the Supplementary material (Section 1).

To investigate the thermal behaviour of the nanocomposite membranes, Thermo Gravimetric Analysis (TGA) and differential scanning

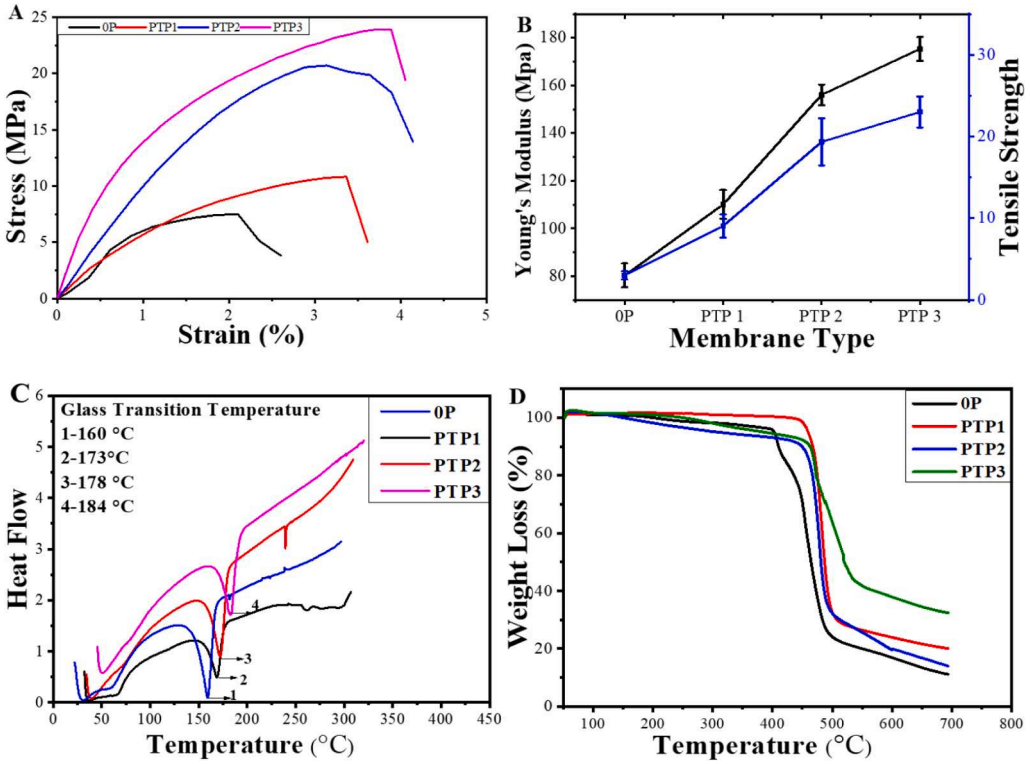

Fig. 5. (A and B) mechanical properties of nanocomposite membrane. (C) Graph of DSC analysis of membranes having different concentrations of TNT's. (D) TGA properties of PVDF-PANI-TNT composite membranes.

calorimetry (DSC) were performed. These analyses were performed to find out the thermal properties such as thermal degradation temperature and glass transition temperature. TGA and DSC of pristine PVDF and PVDF-PANI-TNT nanocomposite membrane with different concentrations of PANI-TNT, i.e. 1% (w/v) to 3% (w/v) are shown in Fig. 5(C, D). Composite membranes were heated from 35°C to 800°C, a considerable weight loss was observed in pure PVDF membrane in comparison to nanocomposite membrane. Thermal degradation temperature of composite membrane rises from 517 °C to 596 °C with addition PANI-TNT nanocomposites [52]. Thermal properties of nanocomposite membrane increase with increase thermal degradation temperature. According to DSC analysis, nanocomposite membranes show a sharp drop in the range of 155–195 °C, which shows the absorption of heat in the sample due to the glass transition temperature of nanocomposite membranes. But in the analysis of nanocomposite membranes with different concentration of PANI-TNT, there is a slight increase in the glass transition temperature. Increase in glass transition temperature is beneficial for our application as it can withstand a higher temperature during the filtration process without degrading the properties [53].

4.5. Membrane permeation properties of PVDF-PANI-TNT nanocomposite membrane

Porosity is voids and empty spaces in the material. The increased porosity results in the higher flow of water from the membrane. The porosity of pure PVDF and nanocomposite membranes were determined by calculating the dry and wet weight of synthesised membrane with water density. Fig. 6(A) illustrate that level of porosity increased with the addition of PANI-TNT nanocomposite from 0 to 3% w/v. The level of porosity increased due to the hydrophilic nature of PANI-TNT content. The oxygen containing functional groups generated on the surface of polyaniline and titania nanotube composite which increases the level of hydrogen bonding with H_2O molecule. It results in enhanced diffusion exchange rate with solvent content (DMF) [31]. The addition of PANI-TNT content also decreases the viscosity of solution, which also enhances the diffusion exchange rate of solvent and increases the porosity [54]. It also had a significant effect on percentage shrinkage ratio. As porosity increases, shrinkage ratio declined due to the enhanced hydrophilic character of the nanocomposite membranes. Fig. 6(A) also represent the percentage shrinkage ratio of nanocomposite membranes which is lower than pure PVDF membrane. It decreases with increasing the concentration of filler (PANI-TNT). It was lower than 13% in nanocomposite membranes which was found to be more effective for membrane filtration.

The hydrophilic properties of pure PVDF and nanocomposite membranes were determined by calculating their contact angle, which plays an important role in the antifouling and pure water flux properties. The hydrophilicity of nanocomposite membranes increased with decrease in contact angle of membrane's surface [55]. When the contact angle of nanocomposite membranes decreased then water molecules easily form a compact layer on the surface of the membrane which repelled organic depositions on their surface and improves its antifouling property. Therefore, this property is beneficial for filtration process to reduce membrane fouling [56,57]. The inclusion of PANI-TNT also introduced —NH group on surface of membrane and formed hydrogen bonding with water molecules which enhanced hydrophilicity of nanocomposite membranes [58]. This evidence is confirmed by the decline in contact angles as illustrated in Fig. 6(B).

To measure the hydrophilic nature of nanocomposite membranes, pure water flux (PWF) was calculated at 0.1 (MPa) pressure. Fig. 6(C) represents the results of pure water flux of developed membranes. PWF of PVDF-PANI-TNT nanocomposite membranes enhances with filler content which demonstrates its hydrophilic nature [59]. Nature of the nanocomposite membranes were determined by four different solvent's polarity. These are arranged as ascending order in polarity from propanol to water. The absorption of solvent in the nanocomposite membranes was calculated by 1 cm^2 of pure PVDF and nanocomposite membranes that were immersed into the various solvents (propanol, methanol, ethanol and water) for 1 day. These were analysed with weight of dry and wet pieces of membrane. The investigated result of

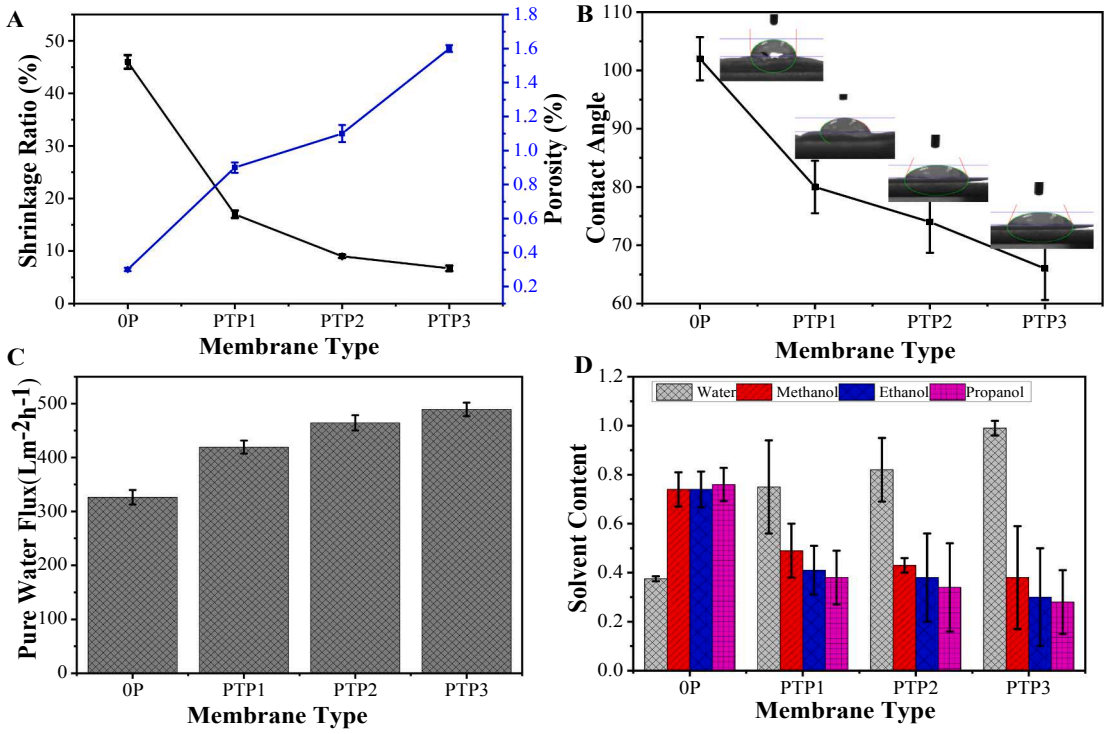

Fig. 6. (A) Graph for shrinkage ratio and porosity synthesised membranes. (B) Contact angle of PVDF-PANI-TNT composite membranes. (C) Pure water flux of composite membranes. (D) Graph showing the variation in solvent contents of composite membranes in different mediums i.e. methanol, ethanol, propanol and water.

solvent contents of these membranes are given in the Fig. 6(D). Results illustrate that the water content within the membrane enhanced with inclusion of filler content (PANI-TNT) and increase the hydrophilic characteristics of nanocomposite membranes. It also increases the water permeability by attracting water molecules towards membrane and facilitated their passage through the nanocomposite membranes.

4.6. Performance of PVDF-PANI-TNT nanocomposite membrane in water purification

4.6.1. Dyes rejection, dye flux and effect of dyes concentration on nanocomposite membrane

Water purification properties of fabricated membranes were determined by two different type of dye solutions (100 ppm) of methyl orange (MO) and allura red (AR) in distilled water. Fig. 7 shows the rejection of dye molecules from contaminated water through PVDF (0P) and nanocomposite membrane (PTP1, PTP2 and PTP3). Dye solutions were passed through the membranes at 0.1 MPa pressure. Dye rejection though membranes was because of the sieving nature of membranes [60]. The molecular weight of these dyes also contributed to the rate of dye rejection, so the same nanocomposite membranes were used to calculate their effect on performance. Results show that with the increase in molecular weight of dyes, the rejection rate was also slightly enhanced [61]. Fig. 7(A, B) illustrate that the nanocomposite membrane PTP3 has a higher dye rejection rate, about 90% for AR and 87% for MO. The hydrodynamic diameter of the two dye molecules are greater than pore size of nanocomposite membranes, so we can say that sieving mechanism of nanocomposite membranes control the flow of contaminated water [62]. Furthermore, the value of dye flux for developed PVDF membrane is less (~324 L m^{-2} h^{-1}), while for nanocomposite membrane (PTP1, PTP2 and PTP3) fluxes are about 407, 439 and 475 (L m^{-2} h^{-1}), respectively. Fig. 7(A, B) represents that efficiency of dye removal through nanocomposite membranes for allura red was greater than methyl orange due to the high molecular weight and different structure of AR dye (496.4 g mol^{-1}) than MO (327.3 $gmol^{-1}$) [63]. Fig. 7 (C) and (D) represents the UV results of permeate solutions of MO and AR from synthesised nanocomposite membrane, respectively. As PANI-TNT content enhanced, the value of UV absorbance of permeate solutions decreases due to excellent dyes filtration capacity of nanocomposite membrane. The insets of Fig. 7(D) and (E) illustrates the solutions after filtration through different membranes (a) PTP3 (b) PTP2 (c) PTP1 and (d) 0P. For reproducibility within the results, mean values are calculated with standard deviation of all experiments. Table 2 provides a detailed comparison of the dyes removal, contact angle and pure water flux of previous research works.

According to the equation of Film Theory [79], different concentrations of dyes in feed solution showed significant effect on nanocomposite membrane performance. Five series of experiments with different concentrations (50–800 ppm) of dyes (MO) were analysed to find their effect on nanocomposite membranes flux and removal of dyes molecule. Fig. 7(C) represent the dye flux of synthesised membrane was gradually decreased with increasing the concentrations of dye feed solutions due to deposition and aggregation effect of dyes molecule onto surface of nanocomposite membrane [80]. Moreover, these deposits and aggregates may block the membrane pores through the adsorption process and increase the fouling on the surface of synthesised membrane. So, the flux of 0P, PTP1, PTP2, PTP3 were decreased by 35.1%, 20.9%, 18.1% and 12.2%, respectively. The slight decline in dye flux of PTP3 nanocomposite membrane illustrates its good antifouling properties [81]. According to Fig. 7(F), dye concentration in feed solution significantly affects dye removal efficiency. Removal efficiency of dyes for nanocomposite membrane PTP3 at 50 mgL^{-1} was less effected and it demonstrate excellent rejection of dye molecules (86%).

4.6.2. Photocatalytic activities under UV light for PVDF-PANI-TNT nanocomposite membranes

According to the preliminary studies, the degradation efficiency of MO for pure PVDF membrane was very low about 0.9% but it increased with the addition of TNTs within nanocomposite membranes. For this purpose, TNTs and PANI were embedded in the structure of the membranes. Photodegradation efficiency of the pure PVDF membrane and nanocomposite membranes (PTP1, PTP2, PTP3) for MO degradation are shown in Fig. 8(A). PTP3 nanocomposite membrane showed excellent photocatalytic activity due to the presence of large number of active sites within the membranes. The kinetics study for MO degradation by PVDF-PANI-TNT nanocomposite membranes were studied according to the kinetic model of Langmuir–Hinshelwood [82]. The rate of the first-order constant was measured through the plot slope of ln (C_o/C_t) and

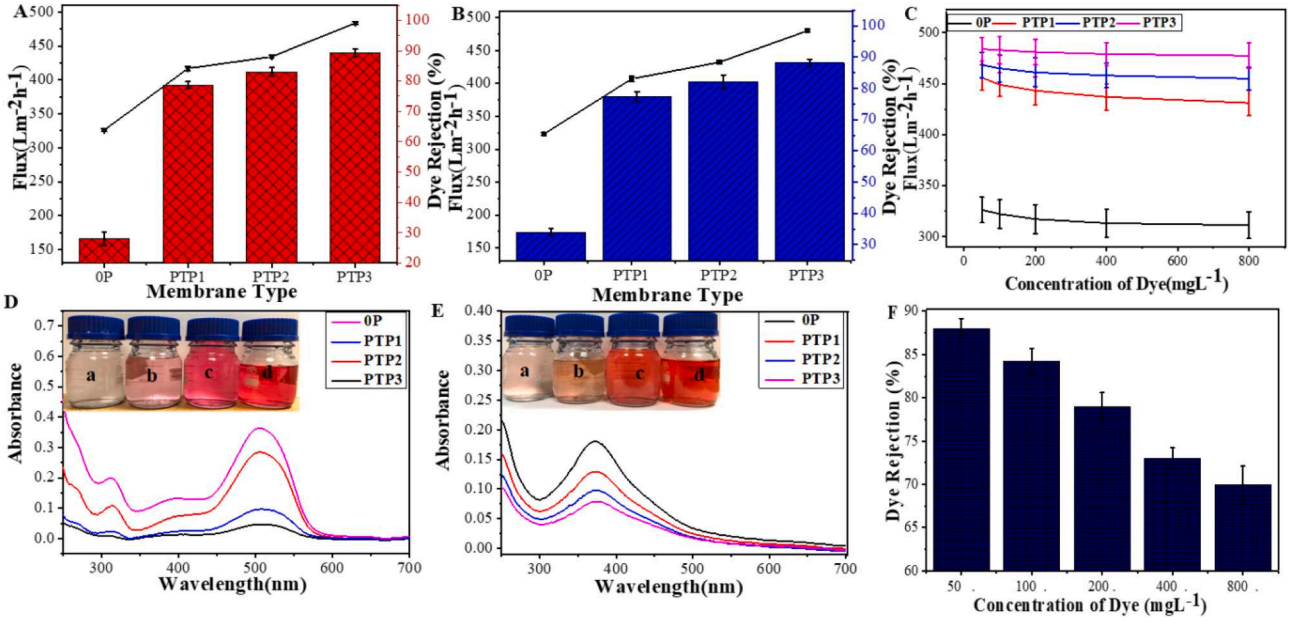

Fig. 7. (A) Dye rejection (Allura Red) and flux of PVDF-PANI-TNT composite membranes. (B) Dye rejection (methyl orange) and flux of PVDF-PANI-TNT composite membranes. (C) Dye concentration effect on dye flux. (D) UV–vis Spectroscopy of Allura Red. (E) UV–vis spectroscopy of methyl orange. (F) Dye concentration effect on dye rejection.

Table 2
Detailed comparison of the dyes removal, contact angle and pure water flux of previous research works.

Membrane Composition	Preparation Method	Water flux (L/m^2 h^1)	Contact Angle	Dyes Rejection (%)	Ref.
PVDF/PVDF-g-POEM	Atom transfer radical polymerization (ATRP)	148	82	77	[64]
PVC/Al_2O_3	–	165	86	89	[65]
PVDF/PAN/ PVA	Extrusion method	201	–	39	[66]
PVDF/PANI	Phase Inversion method	–	65	51	[67]
PES/PEG/PVP	One step electro spinning	212.80	–	81	[68]
Poly(p-phenylene sulfide/GO	Solution casting	325.65	54	94.2	[69]
PVDF-g-PVP	De-fluorination of double bond hydration with graft polymerisation	192.2	71	94	[70]
PS/PES	Interfacial polymerization	35.43	–	90.9	[71]
PVDF/Tetrahydrofuran	Phase inversion	171.80	75	80.3	[72]
PVDF/H_3PO_4	Electrospinning	124.2	84	81	[73]
PAN/ Chitosan	free radical graft copolymerization	229.82	84	89.04	[74]
Polypropylene/PVA	Dip coating method	118.73	62.43	89.2	[75]
Sulfated polyelectrolyte/ Chitosan	Solution casting	110.32	72	79.9	[76]
PVDF/TiO_2	Dip coating	150.3	124	49.2	[77]
Polyamide/carboxyl-functionalized graphene oxide	Interfacial polymerization	311.02	89.32	85	[78]
PVDF/PANI-TiO_2	Phase inversion	484	65.11	90	This Work

irradiation time (t). As represented in Fig. 8(B), the MO degradation by PVDF-PANI-TNT nanocomposite membranes followed first order kinetics reaction. The photocatalytic reaction is also affected by changing pH [83]. To study their effect, the experiments at two different pH values (pH = 3.5 and pH = 9.5) were performed. Fig. 8(C) represents that photodegradation efficiency of the nanocomposite membrane for MO is greater in acidic medium (pH = 3.5) than in basic medium (pH = 9.5). Under alkaline conditions, a large amount of OH^- ions are present in the solution that create the hindrance in the adsorption of organic pollutant on the surface of the nanocomposite membrane. So, it can be concluded that PVDF-PANI-TNT nanocomposite membranes showed good photodegradation activity for MO under a basic medium. Photodegradation rate of PVDF-PANI-TNT nanocomposite membranes for MO at various concentrations of H_2O_2 is shown in Fig. 8(D). It is illustrated that H_2O_2 improved the photocatalytic efficiency of the nanocomposite membrane for MO degradation H_2O_2 was used as a strong oxidant to trap electron generated from polyaniline. Only a specific concentration (less than 1.5 mL) is suitable for photodegradation. Excessive amount slowed down the reaction by the formation of H_2O. Its oxidation is less than oxidation of OH^-.

Fig. 8(E) represent photo degradation activity under UV light for PVDF-PANI-TNT nanocomposite membranes for MO. The performance of filler content (PANI-TNT) within the nanocomposite membrane was significantly more excellent than TNTs or PANI under UV light. Degradation of dye molecules occurs when UV light interact with the catalytic membrane. The energy of molecules within the composite membrane becomes higher than their threshold energies which transferred the electron from the valance band to the conduction band and created a hole into the valance band [84]. These photogenerated induced holes oxidise dye molecules (MO) and degrade them into nontoxic molecules ($CO_2 + H_2O + NH_3 + SO_3^-$). Secondly, the electron in the conduction band reacts with oxygen molecules and generate anion superoxide radical ($O2^-$) which react with dye molecules and degrade them into nontoxic compounds. Fig. 8(E) shows the possible mechanism for the photo degradation of charge carriers on the surface of PVDF-PANI-TNT nanocomposite membranes. Under UV light, polyaniline absorbs light for $\pi \rightarrow \pi^*$ transition, to transport excited-state electrons on the π^* orbital, excited electrons can be transformed into the TiO_2 conduction band, which are transferred on surfaces of membranes. These react with adsorbed water molecule and oxygen molecule to form hydroxyl or superoxide radicals and their holes react with OH^- for the formation of hydroxyl radicals.

4.6.3. BSA rejections and antifouling properties of nanocomposite membrane

Flux of nanocomposite membranes during filtration process declined due to the deposition of solute particles on membrane surface or into the pores of membranes which caused membrane fouling. Although, the fouling on the membrane surface is an unavoidable problem, but it can reduce through useful strategy such as by introducing some hydrophilic filler content into the composition of synthesised membranes. In this study, PANI-TNT nanocomposite was added into the casting solution. As results, it increases the hydrophilic character of nanocomposite membranes and reduced the membrane fouling. The model foulant (BSA) was used to evaluate the antifouling properties of synthesised membranes. Before and after filtration of BSA as feed solutions, pure water flux (PWF) was measured and described as the flux recovery ratio [82]. Fig. 9 (A) illustrate that pure PVDF membrane show hydrophobic characteristics, so it was less effective for BSA rejection (39%) but the rejection rates of nanocomposite membranes (PTP1, PTP2, PTP3) were improved (69%, 73%, 77%, respectively) due to the addition of PANI-TNT nanocomposite [85].

Textile wastewater (solution of methyl orange) was used to evaluate antifouling characteristics and reusability of nanocomposite membranes. The contaminated nanocomposite membranes were washed with anhydrous ethanol and water for 30 min to remove the organic foulant after every cycle, then dried nanocomposite membranes were used for testing reusability of membranes [86]. Fig. 9(B) illustrates that the dye molecules adsorption onto the surface of membrane surface affected the flux of synthesised membrane. With passage of time, dye flux of synthesised membrane was decreased due to the blockage of pores within the membranes. After cleaning for thirty minutes, synthesised membranes show favourable flux recovery within the dye flux of synthesised nanocomposite membranes. Fig. 9(C) represent the FRR of nanocomposite membrane (PTP1, PTP2 and PTP3) was greater in comparison to pristine PVDF membranes after three different cycles. Dye flux for long period of time through synthesised membranes illustrated in Fig. 9(D). Dye flux of synthesised membranes gradually decreased after specific period of time. The decline in flux through PTP3 membrane was less due to the photocatalytic activity of titania nanotubes that can easily degrade dyes molecules present on the surface of membrane [87]. These nanocomposite membranes are hydrophilic in nature. So, they can easily repel hydrophobic contaminant from the membrane surface during water purification process.

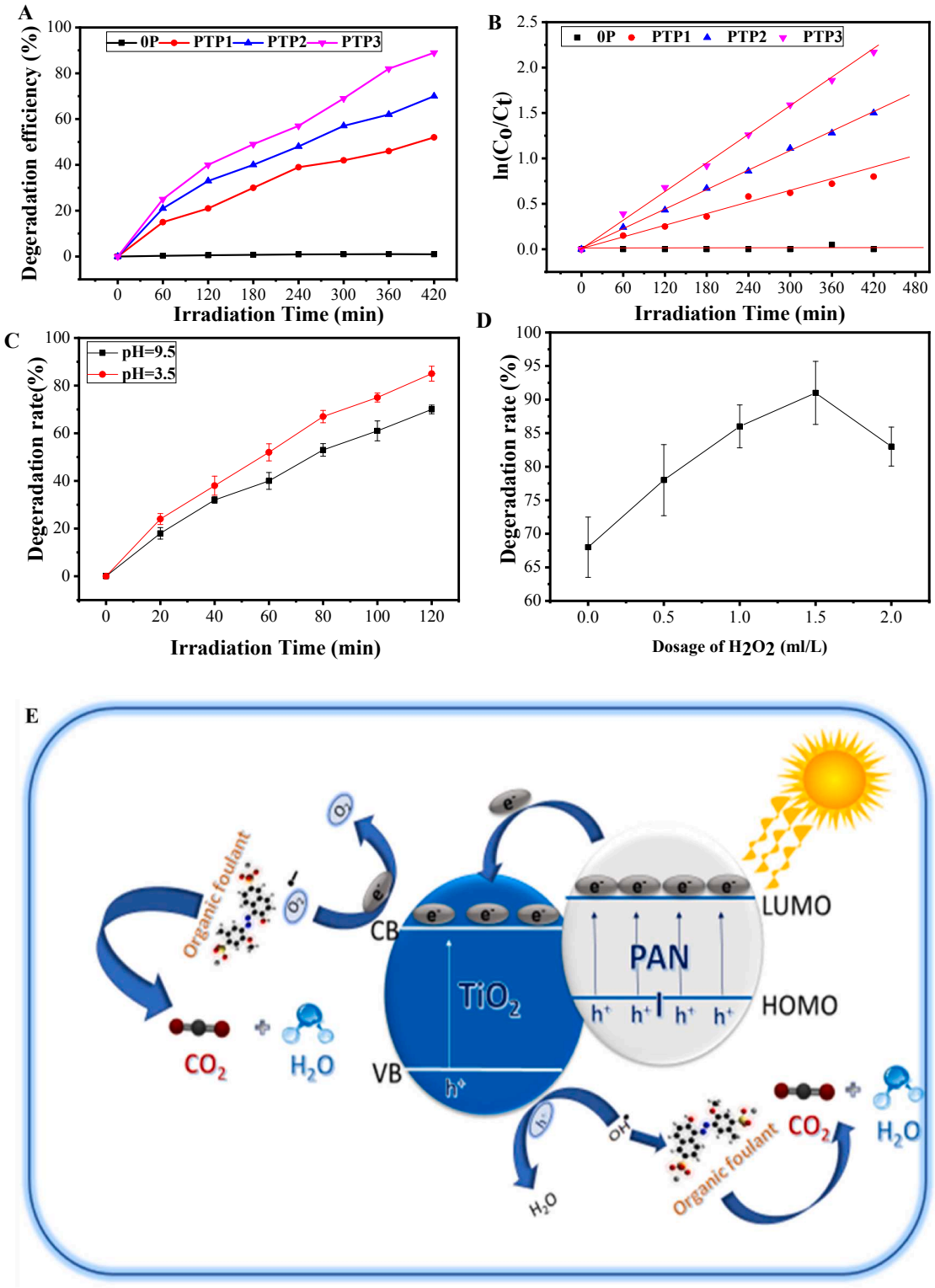

Fig. 8. (A) Degradation efficiency and (B) kinetics of the disappearance of MO by the PVDF-PANI-TNT nanocomposite membranes with different filler content. (C) Degradation rates with irradiation time. (D) Effect of H_2O_2 on degradation rates. (E) An illustration of photocatalytic degradation mechanism of PVDF-PANI-TNT nanocomposite membrane.

5. Conclusion

In our research paper, we explained synthesis process of PANI-TNTs through sol gel process and its composite membrane with PVDF by using the phase inversion methods. The optimised concentration of filler content (PANI-TNT) for water purification membrane is 3% w/v. After the consideration of structural and morphological evidence of synthesised membrane, following conclusions were drawn.

1. The addition of filler content (TNTs and PANI) enhances roughness on surface of composite membrane and improves the hydrophilic properties which decreases the contact angle (from 102.32° to

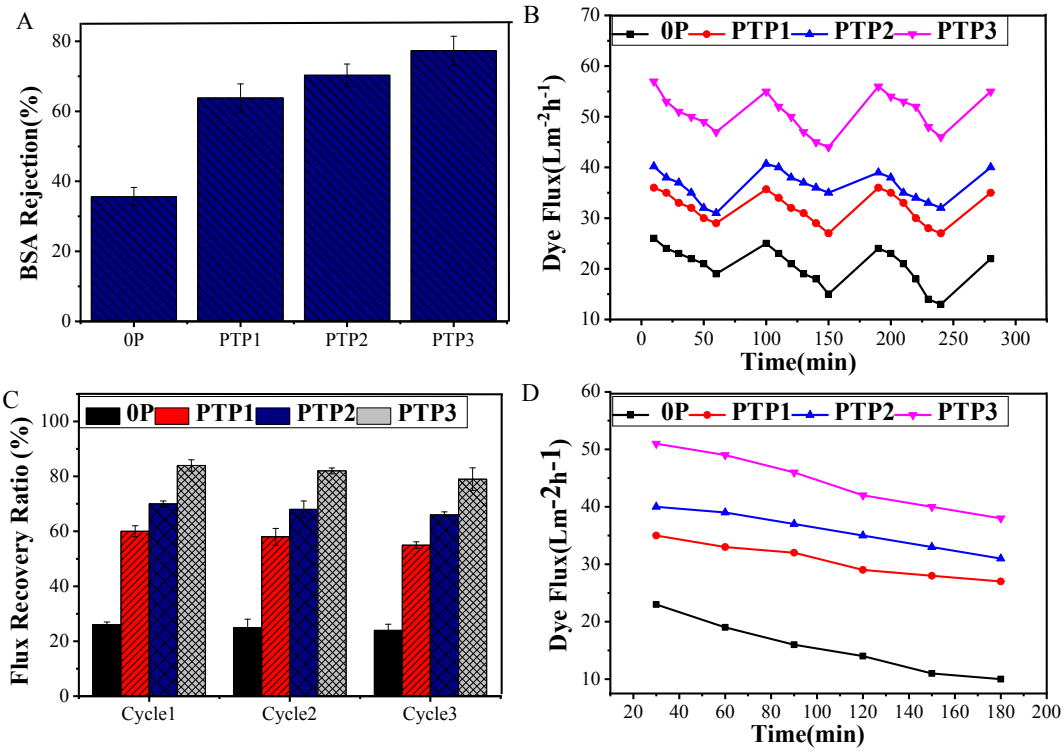

Fig. 9. BSA rejections (A), Capabilities of membrane recycling (B), FRR (C), and Dyes flux (D) of nanocomposite membranes.

66.11°) of nanocomposite membrane. It confirms the presence of oxygen containing functional groups on the surface of nanocomposite membranes.

2. Pore size and shrinkage ratio of PVDF-PANI-TNTs composite membrane are lower in comparison to the developed PVDF membrane. It indicates that filler content improves membrane's permeation properties.
3. Pure water flux of nanocomposite membranes increases from 312 to 484 L m^{-2} h^{-1}. Titania nanotube-polyaniline increases the rate of BSA rejection of nanocomposite membranes from 36.60% to 80.31%.
4. Mechanical and Thermal stability improved with addition (Titania nanotube-polyaniline) composite in synthesised membranes. T_d increase from 517°C to 596 °C and glass transition temperature increase from 15 °C to 195 °C with the inclusion of nanocomposite (PANI-TNT) in pure PVDF membranes. Mechanical properties of nanocomposite membrane also improved by increasing the Young's Modulus from 80.1 (MPa) to 178.03 (MPa).
5. Water purification performance such as BSA rejection, flux recovery ratio and long-term stability of nanocomposite membrane also improved with increment in concentration of fillers (TNTs and PANI).
6. TNTs and PANI composite within the synthesised membrane improve the removal efficiency of dye molecules (AR is 88% and MO is 90%). Synthesised nanocomposite membranes also showed the excellent self-cleaning properties by photocatalytic activity of titania nanotubes.

In view of above discussed conclusions, we can predict that novel PVDF-PANI-TNT nanocomposite membranes have great potential for textile wastewater treatment.

Declaration of Competing Interest

The authors declare that they have no known competing financial interests or personal relationships that could have appeared to influence the work reported in this paper.

Acknowledgements

This research work was supported by grant from Global Challenge Research Fund (GCRF), UK Research Innovation and the Henry Royce Institute for Advanced Materials, funded through EPSRC grants EP/R00661X/1, EP/P025021/1, and EP/P025498/1.

Appendix A. Supplementary data

Supplementary data to this article can be found online at https://doi.org/10.1016/j.cej.2021.129542.

References

[1] J. Zuo, S. Bonyadi, T.S. Chung, Exploring the potential of commercial polyethylene membranes for desalination by membrane distillation, J. Membr. Sci. 497 (2016) 239–247, https://doi.org/10.1016/j.memsci.2015.09.038.
[2] Y. Qin, H. Li, J. Lu, F. Meng, C. Ma, Y. Yan, M. Meng, Nitrogen-doped hydrogenated TiO2 modified with CdS nanorods with enhanced optical absorption, charge separation and photocatalytic hydrogen evolution, Chem. Eng. J. 384 (2020) 123275, https://doi.org/10.1016/j.cej.2019.123275.
[3] G. Zuo, R. Wang, Novel membrane surface modification to enhance anti-oil fouling property for membrane distillation application, J. Membr. Sci. 447 (2013) 26–35, https://doi.org/10.1016/j.memsci.2013.06.053.
[4] Z. Chen, D. Rana, T. Matsuura, Y. Yang, C.Q. Lan, Study on the structure and vacuum membrane distillation performance of PVDF composite membranes: I. Influence of blending, Sep. Purif. Technol. 133 (2014) 303–312, https://doi.org/10.1016/j.seppur.2014.07.015.
[5] J. Lu, Y. Qin, Q. Zhang, C. Yu, Y. Wu, Y. Yan, H. Fan, M. Meng, C. Li, Antibacterial, high-flux and 3D porous molecularly imprinted nanocomposite sponge membranes for cross-flow filtration of emodin from analogues, Chem. Eng. J. 360 (2019) 483–493, https://doi.org/10.1016/j.cej.2018.12.014.
[6] L. Eykens, I. Hitsov, K. De Sitter, C. Dotremont, L. Pinoy, I. Nopens, B. Van der Bruggen, Influence of membrane thickness and process conditions on direct contact membrane distillation at different salinities, J. Membr. Sci. 498 (2016) 353–364, https://doi.org/10.1016/j.memsci.2015.07.037.
[7] I. Galambos, J.M. Molina, P. Jaray, G. Vatai, E.B. Molnar, High organic content industrial wastewater treatment by membrane filtration, Desalination 162 (2005) 117–120. 10.1016/S0011-9164(04)00034-7.
[8] K.h. Krauth, K.F. Staab, Pressurized bioreactor with membrane filtration for wastewater treatment, Water Res. 27 (3) (1993) 405–411, https://doi.org/10.1016/0043-1354(93)90040-O.

[9] E. Dabiri, M. Noori, S. Zahmatkesh, Modeling and CFD simulation of volatile organic compounds removal from wastewater by membrane gas stripping using an electro-spun nanofiber membrane, J. Water Process Eng. 30 (2019) 100635, https://doi.org/10.1016/j.jwpe.2018.05.014.

[10] W. Fuchs, H. Binder, G. Mavrias, R. Braun, Anaerobic treatment of wastewater with high organic content using a stirred tank reactor coupled with a membrane filtration unit, Water Res. 37 (4) (2003) 902–908, https://doi.org/10.1016/S0043-1354(02)00246-4.

[11] D. Hou, G. Dai, H. Fan, J. Wang, C. Zhao, H. Huang, Effects of calcium carbonate nano-particles on the properties of PVDF/nonwoven fabric flat-sheet composite membranes for direct contact membrane distillation, Desalination 347 (2014) 25–33, https://doi.org/10.1016/j.desal.2014.05.028.

[12] M. Modesti, M. Roso, C. Boaretti, S. Besco, D. Hrelja, P. Sgarbossa, A. Lorenzetti, Preparation of smart nano-engineered electrospun membranes for methanol gas-phase photoxidation, Appl. Catal. B Environ. 144 (2014) 216–222, https://doi.org/10.1016/j.apcatb.2013.07.021.

[13] C. Ji, Z. Zhai, C. Jiang, P. Hu, S. Zhao, S. Xue, Z. Yang, T. He, Q.J. Niu, Recent advances in high-performance TFC membranes: a review of the functional interlayers, Desalination 500 (2021) 114869, https://doi.org/10.1016/j.desal.2020.114869.

[14] W. Albrecht, T. Weigel, M. Schossig-Tiedemann, K. Kneifel, K.V. Peinemann, D. Paul, Formation of hollow fiber membranes from poly(ether imide) at wet phase inversion using binary mixtures of solvents for the preparation of the dope, J. Membr. Sci. 192 (2001) 217–230, https://doi.org/10.1016/S0376-7388(01)00504-X.

[15] A. Razmjou, E. Arifin, G. Dong, J. Mansouri, V. Chen, Superhydrophobic modification of TiO 2 nanocomposite PVDF membranes for applications in membrane distillation, J. Membr. Sci. 415–416 (2012) 850–863, https://doi.org/10.1016/j.memsci.2012.06.004.

[16] G.-D. Kang, Y.-M. Cao, Application and modification of poly(vinylidene fluoride) (PVDF) membranes—A review, J. Membr. Sci. 463 (2014) 145–165, https://doi.org/10.1016/j.memsci.2014.03.055.

[17] C. Feng, K.C. Khulbe, S. Tabe, Volatile organic compound removal by membrane gas stripping using electro-spun nanofiber membrane, Desalination 287 (2012) 98–102, https://doi.org/10.1016/j.desal.2011.04.074.

[18] Y. Xiao, X.D. Liu, D.X. Wang, Y.K. Lin, Y.P. Han, X.L. Wang, Feasibility of using an innovative PVDF MF membrane prior to RO for reuse of a secondary municipal effluent, Desalination 311 (2013) 16–23, https://doi.org/10.1016/j.desal.2012.10.022.

[19] X. Chen, S.S. Mao, Titanium dioxide nanomaterials: synthesis, properties, modifications and applications, Chem. Rev. 107 (2007) 2891–2959, https://doi.org/10.1021/cr0500535.

[20] X. Meng, W. Xu, Z. Li, J. Yang, J. Zhao, X. Zou, Y. Sun, Y. Dai, Coupling of hierarchical Al_2O_3/TiO_2 nanofibers into 3D photothermal aerogels toward simultaneous water evaporation and purification, Adv. Fiber Mater. 2 (2) (2020) 93–104, https://doi.org/10.1007/s42765-020-00029-9.

[21] S.J. Oh, N. Kim, Y.T. Lee, Preparation and characterization of PVDF/TiO2 organic-inorganic composite membranes for fouling resistance improvement, J. Membr. Sci. 345 (1-2) (2009) 13–20, https://doi.org/10.1016/j.memsci.2009.08.003.

[22] Y. Sun, J.B. Mwandeje, L.M. Wangatia, F. Zabihi, J. Nedeljković, S. Yang, Enhanced photocatalytic performance of surface-modified TiO_2 nanofibers with rhodizonic acid, Adv. Fiber Mater. 2 (2) (2020) 118–122, https://doi.org/10.1007/s42765-020-00037-9.

[23] X. Cao, J. Ma, X. Shi, Z. Ren, Effect of TiO_2 nanoparticle size on the performance of PVDF membrane, Appl. Surf. Sci. 253 (4) (2006) 2003–2010, https://doi.org/10.1016/j.apsusc.2006.03.090.

[24] Y. Liao, X.G. Li, E.M.V. Hoek, R.B. Kaner, Carbon nanotube/polyaniline nanofiber ultrafiltration membranes, J. Mater. Chem. A. 1 (2013) 15390–15396, https://doi.org/10.1039/c3ta13902f.

[25] Y. Li, Y. Yu, L. Wu, J. Zhi, Processable polyaniline/titania nanocomposites with good photocatalytic and conductivity properties prepared via peroxo-titanium complex catalyzed emulsion polymerization approach, Appl. Surf. Sci. 273 (2013) 135–143, https://doi.org/10.1016/j.apsusc.2013.01.213.

[26] G.R. Guillen, T.P. Farrell, R.B. Kaner, E.M.V. Hoek, Pore-structure, hydrophilicity, and particle filtration characteristics of polyaniline-polysulfone ultrafiltration membranes, J. Mater. Chem. 20 (2010) 4621–4628, https://doi.org/10.1039/b925269j.

[27] S.B. Teli, S. Molina, E.G. Calvo, A.E. Lozano, J. De Abajo, Preparation, characterization and antifouling property of polyethersulfone—PANI/PMA ultra filtration membranes, DES 299 (2012) 113–122, https://doi.org/10.1016/j.desal.2012.05.031.

[28] A.K. Jha, K. Prasad, A.R. Kulkarni, Synthesis of TiO_2 nanoparticles using microorganisms, Colloid. Surf. B 71 (2) (2009) 226–229, https://doi.org/10.1016/j.colsurfb.2009.02.007.

[29] L. Cui, K.N. Hui, K.S. Hui, S.K. Lee, W. Zhou, Z.P. Wan, C.N.H. Thuc, Facile microwave-assisted hydrothermal synthesis of TiO_2 nanotubes, Mater. Lett. 75 (2012) 175–178, https://doi.org/10.1016/j.matlet.2012.02.004.

[30] A. Katoch, M. Burkhart, T. Hwang, S.S. Kim, Synthesis of polyaniline/TiO_2 hybrid nanoplates via a sol-gel chemical method, Chem. Eng. J. 192 (2012) 262–268, https://doi.org/10.1016/j.cej.2012.04.004.

[31] U. Diebold, The surface science of titanium dioxide, Surf. Sci. Rep. 48 (5-8) (2003) 53–229, https://doi.org/10.1016/S0167-5729(02)00100-0.

[32] R.H. Goncalves, W.H. Schreiner, E.R. Leite, Synthesis of TiO_2 nanocrystals with a high affinity for amine organic compounds, Langmuir 26 (14) (2010) 11657–11662, https://doi.org/10.1021/la1007473.

[33] S. Han, L. Mao, T. Wu, H. Wang, Homogeneous polyethersulfone hybrid membranes prepared with in-suit synthesized magnesium hydroxide nanoparticles by phase inversion method, J. Membr. Sci. 516 (2016) 47–55, https://doi.org/10.1016/j.memsci.2016.05.040.

[34] M. Baghbanzadeh, D. Rana, T. Matsuura, C.Q. Lan, Effects of hydrophilic CuO nanoparticles on properties and performance of PVDF VMD membranes, Desalination 369 (2015) 75–84, https://doi.org/10.1016/j.desal.2015.04.032.

[35] T. Iqbal, R. Sahrash, A. Siddiqa, S. Afsheen, M.B. Tahir, M.I. Khan, K.N. Riaz, G. Nabi, M. Fahad, M. Sharif, M. Abrar, Preparation and characterization of polyvinylidene fluoride/1-butyl-3-methylimidazolium bromide-based ionogel membranes for desalination applications, Int. J. Environ. Sci. Technol. 16 (11) (2019) 7081–7092, https://doi.org/10.1007/s13762-019-02207-8.

[36] J. Du, Y.u. Tian, N. Li, J. Zhang, W. Zuo, Enhanced antifouling performance of ZnS/GO/PVDF hybrid membrane by improving hydrophilicity and photocatalysis, Polym. Adv. Technol. 30 (2) (2019) 351–359, https://doi.org/10.1002/pat.v30.210.1002/pat.4472.

[37] S. Goh, J. Zhang, Y. Liu, A.G. Fane, Fouling and wetting in membrane distillation (MD) and MD-bioreactor (MDBR) for wastewater reclamation, Desalination 323 (2013) 39–47, https://doi.org/10.1016/j.desal.2012.12.001.

[38] Y. Orooji, E. Ghasali, N. Emami, F. Noorisafa, A. Razmjou, ANOVA design for the optimization of TiO_2 coating on polyether sulfone membranes, Molecules 24 (2019) 1–13, https://doi.org/10.3390/molecules24162924.

[39] A. Ali, S.U. Ilyas, S. Garg, M. Alsaady, K. Maqsood, R. Nasir, A. Abdulrahman, M. Zulfiqar, A.B. Mahfouz, A. Ahmed, S. Ridha, Dynamic viscosity of titania nanotubes dispersions in ethylene glycol/water-based nanofluids: experimental evaluation and predictions from empirical correlation and artificial neural network, Int. Commun. Heat Mass Transf. 118 (2020) 104882, https://doi.org/10.1016/j.icheatmasstransfer.2020.104882.

[40] Y. Qin, H. Li, J. Lu, Y. Yan, Z. Lu, X. Liu, Enhanced photocatalytic performance of MoS_2 modified by $AgVO_3$ from improved generation of reactive oxygen species, Cuihua Xuebao/Chin. J. Catal. 39 (9) (2018) 1470–1483, https://doi.org/10.1016/S1872-2067(18)63111-0.

[41] M. Sasikumar, N.P. Subiramaniyam, Microstructure, electrical and humidity sensing properties of TiO2/polyaniline nanocomposite films prepared by sol–gel spin coating technique, J. Mater. Sci. Mater. Electron. 29 (9) (2018) 7099–7106, https://doi.org/10.1007/s10854-018-8697-9.

[42] T.T. Van Tran, S.R. Kumar, S.J. Lue, Separation mechanisms of binary dye mixtures using a PVDF ultrafiltration membrane: Donnan effect and intermolecular interaction, J. Membr. Sci. 575 (2019) 38–49, https://doi.org/10.1016/j.memsci.2018.12.070.

[43] X.-L. Cao, Y.-N. Yan, F.-Y. Zhou, S.-P. Sun, Tailoring nanofiltration membranes for effective removing dye intermediates in complex dye-wastewater, J. Membr. Sci. 595 (2020) 117476, https://doi.org/10.1016/j.memsci.2019.117476.

[44] L.u. Yan, S. Hong, M.L. Li, Y.S. Li, Application of the Al_2O_3-PVDF nanocomposite tubular ultrafiltration (UF) membrane for oily wastewater treatment and its antifouling research, Sep. Purif. Technol. 66 (2) (2009) 347–352, https://doi.org/10.1016/j.seppur.2008.12.015.

[45] S. Manna, A.K. Nandi, Piezoelectric β-polymorph in poly (vinylidene fluoride)-functionalized multiwalled carbon nanotube nanocomposite films, J. Phys. Chem. C. 111 (2007) 14670–14680. 10.1021/jp073102l.

[46] N. Meng, R.C.E. Priestley, Y. Zhang, H. Wang, X. Zhang, The effect of reduction degree of GO nanosheets on microstructure and performance of PVDF/GO hybrid membranes, J. Memb. Sci. 501 (2016) 169–178, https://doi.org/10.1016/j.memsci.2015.12.004.

[47] S.G. Pawar, S.L. Patil, M.A. Chougule, A.T. Mane, D.M. Jundale, V.B. Patil, Synthesis and characterization of polyaniline:TiO_2 nanocomposites, Int. J. Polym. Mater. Polym. Biomater. 59 (10) (2010) 777–785, https://doi.org/10.1080/00914037.2010.483217.

[48] J. Lu, Y. Qin, Y. Wu, M. Meng, Z. Dong, C. Yu, Y. Yan, C. Li, F.K. Nyarko, Bidirectional molecularly imprinted membranes for selective recognition and separation of pyrimethamine: a double-faced loading strategy, J. Membr. Sci. 601 (2020) 117917, https://doi.org/10.1016/j.memsci.2020.117917.

[49] J. Lu, Y. Qin, C. Li, Y. Wu, M. Meng, Z. Dong, C. Sun, M. Chen, Y. Yan, Irregular dot array nanocomposite molecularly imprinted membranes with enhanced antibacterial property: Synergistic promotion of selectivity, rebinding capacity and flux, Chem. Eng. J. 405 (2021) 126716, https://doi.org/10.1016/j.cej.2020.126716.

[50] J. Zuo, T.S. Chung, G.S. O'Brien, W. Kosar, Hydrophobic/hydrophilic PVDF/Ultem® dual-layer hollow fiber membranes with enhanced mechanical properties for vacuum membrane distillation, J. Membr. Sci. 523 (2017) 103–110, https://doi.org/10.1016/j.memsci.2016.09.030.

[51] J. Zhang, Z. Xu, W. Mai, C. Min, B. Zhou, M. Shan, Y. Li, C. Yang, Z. Wang, X. Qian, Improved hydrophilicity, permeability, antifouling and mechanical performance of PVDF composite ultrafiltration membranes tailored by oxidized low-dimensional carbon nanomaterials, J. Mater. Chem. A. 1 (2013) 3101–3111, https://doi.org/10.1039/c2ta01415g.

[52] Y. Zhang, Y. Peng, S. Ji, Z. Li, P. Chen, Review of thermal efficiency and heat recycling in membrane distillation processes, Desalination 367 (2015) 223–239, https://doi.org/10.1016/j.desal.2015.04.013.

[53] M.O. Ansari, F. Mohammad, Thermal stability, electrical conductivity and ammonia sensing studies on p-toluenesulfonic acid doped polyaniline: Titanium dioxide (pTSA/Pani:TiO 2) nanocomposites, Sens. Actuat. B Chem. 157 (1) (2011) 122–129, https://doi.org/10.1016/j.snb.2011.03.036.

[54] J. Zhang, Z. Wang, Q. Wang, J. Ma, J. Cao, W. Hu, Z. Wu, Relationship between polymers compatibility and casting solution stability in fabricating PVDF/PVA

membranes, J. Membr. Sci. 537 (2017) 263–271, https://doi.org/10.1016/j.memsci.2017.05.041.
[55] X. Chen, Y. He, Y. Fan, G. Zeng, L. Zhang, Nature-inspired polyphenol chemistry to fabricate halloysite nanotubes decorated PVDF membrane for the removal of wastewater, Sep. Purif. Technol. 212 (2019) 326–336, https://doi.org/10.1016/j.seppur.2018.11.036.
[56] X. Chang, Z. Wang, S. Quan, Y. Xu, Z. Jiang, L. Shao, Exploring the synergetic effects of graphene oxide (GO) and polyvinylpyrrodione (PVP) on poly (vinylylidenefluoride) (PVDF) ultrafiltration Membrane performance, Appl. Surf. Sci. 316 (2014) 537–548, https://doi.org/10.1016/j.apsusc.2014.07.202.
[57] B.M. Ganesh, A.M. Isloor, A.F. Ismail, Enhanced hydrophilicity and salt rejection study of graphene oxide-polysulfone mixed matrix membrane, Desalination 313 (2013) 199–207, https://doi.org/10.1016/j.desal.2012.11.037.
[58] G. Whyman, E. Bormashenko, T. Stein, The rigorous derivation of Young, Cassie-Baxter and Wenzel equations and the analysis of the contact angle hysteresis phenomenon, Chem. Phys. Lett. 450 (4-6) (2008) 355–359, https://doi.org/10.1016/j.cplett.2007.11.033.
[59] D. Sun, M.Q. Liu, J.H. Guo, J.Y. Zhang, B.B. Li, D.Y. Li, Preparation and characterization of PDMS-PVDF hydrophobic microporous membrane for membrane distillation, Desalination 370 (2015) 63–71, https://doi.org/10.1016/j.desal.2015.05.017.
[60] M. Amini, M. Arami, N.M. Mahmoodi, A. Akbari, Dye removal from colored textile wastewater using acrylic grafted nanomembrane, Desalination 267 (1) (2011) 107–113, https://doi.org/10.1016/j.desal.2010.09.014.
[61] R. Han, S. Zhang, D. Xing, X. Jian, Desalination of dye utilizing copoly (phthalazinone biphenyl ether sulfone) ultrafiltration membrane with low molecular weight cut-off, J. Membr. Sci. 358 (1-2) (2010) 1–6, https://doi.org/10.1016/j.memsci.2010.03.036.
[62] M.E. Lydon, K.A. Unocic, T.-H. Bae, C.W. Jones, S. Nair, Structure-property relationships of inorganically surface-modified zeolite molecular sieves for nanocomposite membrane fabrication, J. Phys. Chem. C. 116 (17) (2012) 9636–9645, https://doi.org/10.1021/jp301497d.
[63] Y. Zhao, W. Yu, R. Li, Y. Xu, Y. Liu, T. Sun, L. Shen, H. Lin, Electric field endowing the conductive polyvinylidene fluoride (PVDF)-graphene oxide (GO)-nickel (Ni) membrane with high-efficient performance for dye wastewater treatment, Appl. Surf. Sci. 483 (2019) 1006–1016, https://doi.org/10.1016/j.apsusc.2019.04.054.
[64] A. Akthakul, R.F. Salinaro, A.M. Mayes, Antifouling polymer membranes with subnanometer size selectivity, Macromolecules 37 (20) (2004) 7663–7668, https://doi.org/10.1021/ma048837s.
[65] P. Chen, X. Ma, Z. Zhong, F. Zhang, W. Xing, Y. Fan, Performance of ceramic nanofiltration membrane for desalination of dye solutions containing NaCl and Na2SO4, Desalination 404 (2017) 102–111, https://doi.org/10.1016/j.desal.2016.11.014.
[66] K. Karakulski, W.A. Morawski, J. Grzechulska, Purification of bilge water by hybrid ultrafiltration and photocatalytic processes, Sep. Purif. Technol. 14 (1-3) (1998) 163–173, https://doi.org/10.1016/S1383-5866(98)00071-9.
[67] C.H. Nguyen, C.C. Fu, D.Y. Kao, T.T. Van Tran, R.S. Juang, Adsorption removal of tetracycline from water using poly(vinylidene fluoride)/polyaniline-montmorillonite mixed matrix membranes, J. Taiwan Inst. Chem. Eng. 112 (2020) 259–270, https://doi.org/10.1016/j.jtice.2020.06.007.
[68] J. Gao, Z. Thong, K. Yu Wang, T.S. Chung, Fabrication of loose inner-selective polyethersulfone (PES) hollow fibers by one-step spinning process for nanofiltration (NF) of textile dyes, J. Membr. Sci. 541 (2017) 413–424, https://doi.org/10.1016/j.memsci.2017.07.016.
[69] Y. Gao, K. Su, X. Wang, Z. Li, A metal-nano GO frameworks/PPS membrane with super water flux and high dyes interception, J. Membr. Sci. 574 (2019) 55–64, https://doi.org/10.1016/j.memsci.2018.12.052.
[70] X. Huang, W. Wang, Y. Liu, H. Wang, Z. Zhang, W. Fan, L. Li, Treatment of oily waste water by PVP grafted PVDF ultrafiltration membranes, Chem. Eng. J. 273 (2015) 421–429, https://doi.org/10.1016/j.cej.2015.03.086.
[71] X. Wei, X. Kong, C. Sun, J. Chen, Characterization and application of a thin-film composite nanofiltration hollow fiber membrane for dye desalination and concentration, Chem. Eng. J. 223 (2013) 172–182, https://doi.org/10.1016/j.cej.2013.03.021.
[72] M. Mertens, T. Van Dyck, C. Van Goethem, A.Y. Gebreyohannes, I.F.J. Vankelecom, Development of a polyvinylidene difluoride membrane for nanofiltration, J. Membr. Sci. 557 (2018) 24–29, https://doi.org/10.1016/j.memsci.2018.04.020.
[73] D. Hou, G. Dai, J. Wang, H. Fan, L. Zhang, Z. Luan, Preparation and characterization of PVDF/nonwoven fabric flat-sheet composite membranes for desalination through direct contact membrane distillation, Sep. Purif. Technol. 101 (2012) 1–10, https://doi.org/10.1016/j.seppur.2012.08.031.
[74] S. Liu, Z. Wang, P. Song, Free radical graft copolymerization strategy to prepare catechin-modified chitosan loose nanofiltration (NF) membrane for dye desalination, ACS Sustain. Chem. Eng. 6 (3) (2018) 4253–4263, https://doi.org/10.1021/acssuschemeng.7b04699.
[75] Y. Zheng, G. Yao, Q. Cheng, S. Yu, M. Liu, C. Gao, Positively charged thin-film composite hollow fiber nanofiltration membrane for the removal of cationic dyes through submerged filtration, Desalination 328 (2013) 42–50, https://doi.org/10.1016/j.desal.2013.08.009.
[76] C.C. Ye, F.Y. Zhao, J.K. Wu, X.D. Weng, P.Y. Zheng, Y.F. Mi, Q.F. An, C.J. Gao, Sulfated polyelectrolyte complex nanoparticles structured nanoflitration membrane for dye desalination, Chem. Eng. J. 307 (2017) 526–536, https://doi.org/10.1016/j.cej.2016.08.122.
[77] L. Penboon, A. Khrueakham, S. Sairiam, TiO_2 coated on PVDF membrane for dye wastewater treatment by a photocatalytic membrane, Water Sci. Technol. 79 (2019) 958–966, https://doi.org/10.2166/wst.2019.023.
[78] H. Zhang, Bin Li, J. Pan, Y. Qi, J. Shen, C. Gao, B. Van der Bruggen, Van der Bruggen, Carboxyl-functionalized graphene oxide polyamide nanofiltration membrane for desalination of dye solutions containing monovalent salt, J. Membr. Sci. 539 (2017) 128–137, https://doi.org/10.1016/j.memsci.2017.05.075.
[79] I. Koyuncu, D. Topacik, M.R. Wiesner, Factors influencing flux decline during nanofiltration of solutions containing dyes and salts, Water Res. 38 (2) (2004) 432–440, https://doi.org/10.1016/j.watres.2003.10.001.
[80] N.M. Mokhtar, W.J. Lau, A.F. Ismail, W. Youravong, W. Khongnakorn, K. Lertwittayanon, Performance evaluation of novel PVDF-Cloisite 15A hollow fiber composite membranes for treatment of effluents containing dyes and salts using membrane distillation, RSC Adv. 5 (48) (2015) 38011–38020, https://doi.org/10.1039/C5RA00182J.
[81] I. Koyuncu, Reactive dye removal in dye/salt mixtures by nanofiltration membranes containing vinylsulphone dyes: Effects of feed concentration and cross flow velocity, Desalination 143 (3) (2002) 243–253, https://doi.org/10.1016/S0011-9164(02)00263-1.
[82] K.J. Lu, J. Zuo, T.S. Chung, Novel PVDF membranes comprising n-butylamine functionalized graphene oxide for direct contact membrane distillation, J. Membr. Sci. 539 (2017) 34–42, https://doi.org/10.1016/j.memsci.2017.05.064.
[83] Y. Qin, H. Li, J. Lu, Y. Feng, F. Meng, C. Ma, Y. Yan, M. Meng, Synergy between van der waals heterojunction and vacancy in ZnIn2S4/g-C3N4 2D/2D photocatalysts for enhanced photocatalytic hydrogen evolution, Appl. Catal. B Environ. 277 (2020) 119254, https://doi.org/10.1016/j.apcatb.2020.119254.
[84] R. Kumar, M.O. Ansari, N. Parveen, M. Oves, M.A. Barakat, A. Alshahri, M.Y. Khan, M.H. Cho, Facile route to a conducting ternary polyaniline@TiO_2/GN nanocomposite for environmentally benign applications: photocatalytic degradation of pollutants and biological activity, RSC Adv. 6 (112) (2016) 111308–111317, https://doi.org/10.1039/C6RA24079H.
[85] S. Gul, Z.A. Rehan, S.A. Khan, K. Akhtar, M.A. Khan, M.I. Khan, M.I. Rashid, A. M. Asiri, S.B. Khan, Antibacterial PES-CA-Ag_2O nanocomposite supported Cu nanoparticles membrane toward ultrafiltration, BSA rejection and reduction of nitrophenol, J. Mol. Liq. 230 (2017) 616–624, https://doi.org/10.1016/j.molliq.2016.12.093.
[86] M. Isoyama, S. Wada, Remediation of Pb-contaminated soils by washing with hydrochloric acid and subsequent immobilization with calcite and allophanic soil, J. Hazard. Mater. 143 (3) (2007) 636–642, https://doi.org/10.1016/j.jhazmat.2007.01.008.
[87] J. Lin, W. Ye, H. Zeng, H. Yang, J. Shen, S. Darvishmanesh, P. Luis, A. Sotto, B. Van der Bruggen, Fractionation of direct dyes and salts in aqueous solution using loose nanofiltration membranes, J. Membr. Sci. 477 (2015) 183–193.